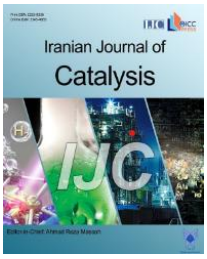

Iran. J. Catal. 2026; 16(1): 50-60

Iranian Journal of Catalysis (IJC)

https://doi.org/10.57647/ijc.2026.1601.04

Research Article

Iron Catalysed Decarboxylative Oxidation Photocatalysis of Alpha-Carbon to Access Aldehyde/Ketone from Aryl Aliphatic Carboxylic Acid

Raunak Katiyar, Sumit Kumar, Gopal L. Khatik*

Department of Medicinal Chemistry, National Institute of Pharmaceutical Education and Research-Raebareli, Uttar Pradesh, India

*Corresponding authors: gopal.khatik@niperraebareli.edu.in, gopal_niper@rediffmail.com

Article History:

Received:
18 August 2025

Revised:
15 October 2025

Accepted:
04 November 2025

Published Online:
25 November 2025

Published in Issue:
31 March 2026

Abstract

Carbonyl-containing compounds, such as aldehydes and ketones, are fundamental to synthetic organic chemistry, with wide-ranging applications in the pharmaceutical industry. In this study, we introduce an efficient and streamlined metallophotoredox approach for decarboxylative oxygenation via visible-light-induced ligand-to-metal charge transfer (LMCT). Our method simplifies the transformation of aryl aliphatic carboxylic acids into their corresponding aryl aldehydes and ketones, utilizing iron(III) triflate as a photo catalyst in the presence of TMEDA as a ligand. This strategy not only enhances environmental sustainability but also expands the potential for late-stage functionalization of complex molecules and bioactive compounds.

Keywords: Aldehyde; Carboxylic acid; Decarboxylative oxygenation; Iron (III) triflate; Ketone; Metallophotoredox

Cite this article: R. Katiyar, S. Kumar, G. L. Khatik, Iran. J. Catal. **16** (2026) 50-60. https://doi.org/10.57647/ijc.2026.1601.04

1. Introduction

The decarboxylation is a key transformation with broad significance in both chemical biology and organic synthesis. Carbonyl-containing organic frameworks, such as aldehydes and ketones, play a crucial role in synthetic organic chemistry across both academic research and industrial applications [1].

Aldehydes are important in organic synthesis and are useful precursors for various industries, including fragrances, pharmaceuticals, and food industries [2]. Metallophotoredox catalysis is a rapidly growing field that enables efficient and useful methods for driving a wide range of organic reactions.

Usages of photo redox catalysts containing late transition metals like iridium and ruthenium are facing challenges due to their high cost and limited availability. Some of the iron catalysts are already being reported for the benzylic oxygenation [3] and chemo and regioselective alkene oxidation [4] by thiyl radical generation.

This highlights the potential benefits of exploring earth-abundant metal catalysts like iron [5].

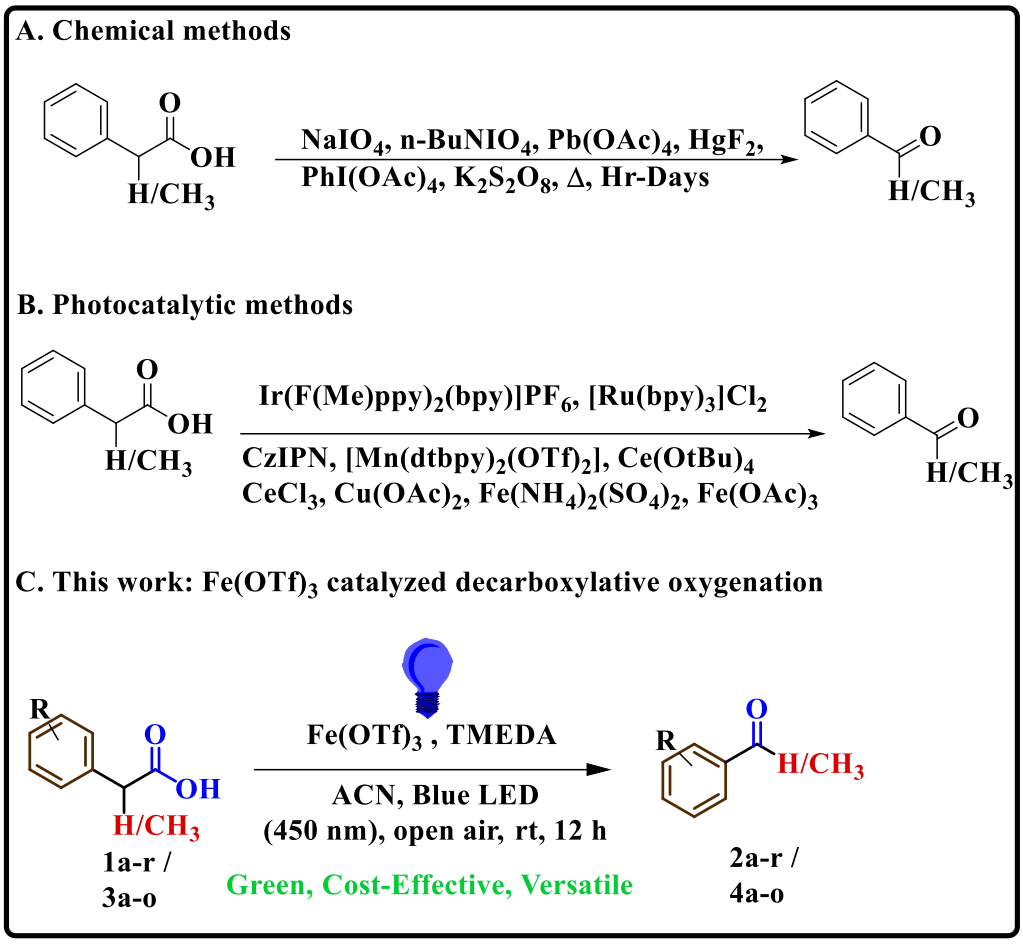

Scheme 1. Decarboxylative Oxygenation

Traditional decarboxylative strategies have often relied on stoichiometric amounts of harsh oxidants such as $Pb(OAc)_4$ [6], $K_2S_2O_8$ [7], $PhI(OAc)_2$ [8], or metal-based reagents like HgF_2 [9], and $NaIO_4$ [10], which pose limitations due to toxicity, poor atom economy, and reduced functional group tolerance (Scheme 1A).

Additionally, many of these protocols require elevated temperatures or inert conditions, which further restrict their synthetic utility. In contrast, recent advancements have showcased visible-light-mediated oxidative decarboxylation as a sustainable alternative, employing molecular oxygen (O_2) as a terminal oxidant. Usages of photo redox catalysts containing late transition metals like ruthenium[11] and iridium [12] is facing challenges due to its high cost and limited availability.

These methodologies leverage metallophotoredox catalysts such as $[Ru(bpy)_3]$ Cl_2 [11], $[Ir(F(Me)ppy)_2(bpy)]PF_6$ [12], $Ce(OtBu)_4$ [13], $Fe(OAc)_3$ [14], $Cu(OAc)_2$ [15], to promote ligand-to-metal (LMCT) or metal-to-ligand charge transfer (MLCT) pathways under mild conditions (Scheme 1B). These approaches not only offer improved environmental compatibility but also broaden the scope for late-stage functionalization of bioactive molecules and complex scaffolds [16]. Herein, our method employs the cost-effective and easily available TMEDA and ferric triflate catalyst, which has a good yield and is easily purified since the catalyst and ligands are water soluble.

2. Experimental

2.1. General information

All reactions were conducted under ambient air unless otherwise specified. Reagents were used as received from commercial suppliers, including Sigma-Aldrich, Spectrochem Pvt. Ltd., Sisco Research Laboratories Pvt. Ltd., Agnitio, GLR Innovation, and Labogen, or were synthesized in-house, without further purification. Visible light irradiation was provided by high-power LED modules (10 W, ~450 nm) sourced from Torpe Computer Service. Reaction progress was monitored by thin-layer chromatography (TLC) using Merck pre-coated silica gel plates (60 F254, 0.25 mm thickness), with visualization under UV light. Nuclear magnetic resonance (NMR) spectra were recorded on a JEOL RESONANCE ECZ500R spectrometer at 500 MHz for ^1H NMR and 125 MHz for ^{13}C NMR in DMSO-d_6, using tetramethylsilane (TMS) as the internal standard. Chemical shifts are reported in parts per million (ppm), and coupling constants are given in Hertz (Hz). Splitting patterns are denoted as singlet (s), doublet (d), triplet (t), multiplet (m),

10.57647/ijc.2026.1601.04

doublet of doublet (dd), and doublet of triplet (dt). High-resolution mass spectrometry (HRMS) analyses were performed using an electrospray ionization (ESI) quadrupole time-of-flight (QTOF) mass spectrometer (Agilent Technologies).

2.2. Reaction set up

The decarboxylative oxygenation reactions were conducted in a custom-designed enclosure equipped with a 10 W blue LED module (~450 nm, Thorpe Computer Service) as the primary light source for photoactivation. To regulate thermal load and ensure sufficient airflow, a V-Guard Spinny Pro multipurpose personal fan, delivering an air flow rate of 353 m^3/min at 2100 RPM, was mounted on the upper side of the enclosure. Additionally, the lower side of the enclosure was designed with open ventilation space to facilitate continuous air exchange and prevent overheating.

2.3. General procedure of synthesis (2a-r and 4a-o)

An oven-dried Schlenk tube was charged with Iron (III) triflate (0.036 g, 10 mol%, 0.10 equiv), TMEDA (0.012 g, 0.016 ml, 15 mol%, 0.15 equiv), and phenylacetic acid (0.1 g, 0.7 mmol, 1 equiv.) in 3 mL of acetonitrile. The reaction mixture was stirred in an open and irradiated with a 10 W blue LED (~450 nm) for 12 hours. Upon completion, the reaction mixture was worked up by extraction with ethyl acetate and water. The combined organic layers were dried over anhydrous sodium sulfate and concentrated under reduced pressure to get the product.

Benzaldehyde (2a): 0.054g; Yield 70%; transparent liquid; ^{1}H NMR (500 MHz, DMSO-d_6) (δ ppm): 9.96 (s, 1H), 7.85 (d, J = 8.2 Hz, 2H), 7.69 – 7.59 (m, 1H), 7.53 (t, J = 6.8 Hz, 2H); ^{13}C NMR (125 MHz, DMSO-d_6) (δ ppm): 193.64, 136.71, 135.03, 129.98, 129.61.

4-Fluorobenzaldehyde (2b): 0.055g; Yield 69%; transparent liquid; ^{1}H NMR (500 MHz, DMSO-d_6) (δ ppm): 9.93 (s, 1H), 7.94 (dd, J = 7.9, 5.7 Hz, 2H), 7.37 (t, J = 8.9 Hz, 2H); ^{13}C NMR (125 MHz, DMSO-d_6) (δ ppm): 192.08, 166.28 (d, ^1J = 253.5 Hz), 133.58, 132.85 (d, ^3J = 9.7 Hz), 116.83 (d, ^2J = 22.3 Hz).

3-Chlorobenzaldehyde (2c): 0.062g; Yield 76%; transparent liquid; ^{1}H NMR (500 MHz, DMSO- d_6) (δ ppm): 9.86 (s, 1H), 7.83 – 7.73 (m, 2H), 7.64 (s, 1H), 7.51-7.55 (m, 1H); ^{13}C NMR (125 MHz, DMSO- d_6) (δ ppm): 192.99, 138.14, 134.79, 134.64, 131.66, 129.26, 128.60.

4-Chlorobenzaldehyde (2d): 0.058g; Yield 73%; white solid; ^{1}H NMR (500 MHz, DMSO- d_6) (δ ppm): 9.96 (s, 1H), 7.89 (d, J = 8.0 Hz, 2H), 7.65 (d, J = 8.3 Hz, 2H); ^{13}C NMR (125 MHz, DMSO- d_6) (δ ppm): 192.61,139.91, 135.39, 131.72, 129.91.

2,4-dichlorobenzaldehyde (2e): 0.059g; Yield 70%; transparent liquid; ^{1}H NMR (500 MHz, DMSO- d_6) (δ ppm): 10.21 (s, 1H), 7.79 (d, J = 8.3 Hz, 1H), 7.71 (s, 1H), 7.54 (d, J = 8.3 Hz, 1H); ^{13}C NMR (125 MHz, DMSO-d_6) (δ **ppm):** 189.25, 140.28, 137.67, 131.52, 131.44, 130.75, 128.78.

3-Bromobenzaldehyde (2f): 0.056g; Yield 66%; yellow liquid; ^{1}H NMR (500 MHz, DMSO- d_6) (δ ppm): 9.91 (s, 1H), 7.94 (s, 1H), 7.81 (d, J = 7.5 Hz, 1H), 7.76 (d, J = 8.0 Hz, 1H), 7.46 (t, J = 7.8 Hz, 1H); ^{13}C NMR (125 MHz, DMSO- d_6) (δ ppm): 192.25, 138.50, 137.45, 132.38, 131.70, 128.75, 122.99.

4-Bromobenzaldehyde (2g): 0.053g; Yield 62%; Yellow solid ^{1}H NMR (500 MHz, DMSO- d_6) (δ ppm): 9.95 (s, 1H), 7.79 (d, J = 8.7 Hz, 2H), 7.75 (d, J = 8.7 Hz, 2H); ^{13}C NMR (125 MHz, DMSO- d_6 (δ ppm): 192.91,135.64, 132.84, 131.78, 129.23

4-Trifluoromethyl benzaldehyde (2h): 0.061g; Yield 72%; transparent liquid; ^{1}H NMR (500 MHz, DMSO- d_6) (δ ppm): 10.09 (s, 1H), 8.06 (d, J = 8.1 Hz, 2H), 7.87 (d, J = 8.3 Hz, 2H). ^{13}C NMR (125 MHz, DMSO- d_6) (δ ppm): 193.24, 139.63, 134.35 (q, $1J_{CF3}$ = 31.9 Hz), 130.49, 126.46 124.16 (q, $2J_{CF3}$ = 272.9 Hz),120.90.

4-Nitrobenzaldehyde (2i): 0.053g; Yield 64%; white solid; ^{1}H NMR (500 MHz, DMSO- d_6) (δ ppm): 10.11 (s, 1H), 8.36 (d, J = 8.9 Hz, 2H), 8.11 (d, J = 8.9 Hz, 2H); ^{13}C NMR (125 MHz, DMSO- d_6) (δ ppm): 192.87, 151.15, 140.59, 131.17, 124.80.

4-Cyanobenzaldehyde (2j): 0.053g; Yield 66%; light yellow solid; ^{1}H NMR (500 MHz, DMSO- d_6) (δ ppm): 10.06 (s, 1H), 8.03 (s, 4H). ^{13}C NMR (125 MHz, DMSO-d_6) (δ ppm): 193.12, 139.30, 133.71, 130.40, 118.61, 116.74.

4-Hydroxybenzaldehyde (2k): 0.062g; Yield 78%; cream solid; ^{1}H NMR (500 MHz, DMSO- d_6) (δ ppm): 10.59 (s, 1H), 9.75 (s, 1H), 7.72 (d, J = 7.3 Hz, 2H), 6.90 (d, J = 7.3 Hz, 2H); ^{13}C NMR (125 MHz, DMSO- d_6) (δ ppm): 191.44, 163.90, 132.63, 128.95, 116.32.

3,4-dihydroxybenzaldehyde (2l): 0.055g; Yield 68%; brownish solid; ^{1}H NMR (500 MHz, DMSO- d_6) (δ ppm): 10.02 (s, 1H), 9.66 (s, 1H), 9.46 (s, 1H), 7.23 (d, J = 8.0 Hz, 1H), 7.20 (s, 1H), 6.87 (d, J = 8.9 Hz, 1H); ^{13}C NMR (125 MHz, DMSO- d_6) (δ ppm): 191.64, 152.67, 146.43, 129.38, 125.04, 116.06, 114.88.

4-Methoxybenzaldehyde (2m): 0.062g; Yield 76%; light yellow liquid; ^{1}H NMR (500 MHz, DMSO- d_6) (δ ppm):

9.80 (s, 1H), 7.79 (d, *J* = 9.0 Hz, 2H), 7.02 (d, *J* = 8.9 Hz, 2H), 3.77 (s, 3H); ^{13}C NMR (125 MHz, DMSO- *d*$_6$) (δ ppm): 191.59, 164.71, 132.23, 130.17, 114.87, 55.99.

3,4-dimethoxybenzaldehyde (2n): 0.056g; Yield 67%; white solid; ^{1}H NMR (500 MHz, DMSO- *d*$_6$) (δ ppm): 9.80 (s, 1H), 7.52 (d, *J* = 8.2 Hz, 1H), 7.34 (s, 1H), 7.13 (d, *J* = 8.3 Hz, 1H), 3.88 (s, 3H), 3.78 (s, 3H); ^{13}C NMR (125 MHz, DMSO- *d*$_6$) (δ ppm): 191.89, 154.72, 149.69, 130.17, 126.61, 111.77, 109.94, 56.38, 56.01.

3,4,5-Trimethoxybenzaldehyde (2o): 0.058g; Yield 68%; pale yellow solid; ^{1}H NMR (500 MHz, DMSO- *d*$_6$) (δ ppm): 9.81 (s, 1H), 7.18 (s, 2H), 3.81 (s, 6H), 3.72 (s, 3H); ^{13}C NMR (125 MHz, DMSO- *d*$_6$) (δ ppm): 192.31, 154.31, 143.36, 132.17, 107.20, 60.68, 56.50.

4-Methyl benzaldehyde (2p): 0.061g; Yield 77%; transparent liquid; ^{1}H NMR (500 MHz, DMSO- *d*$_6$) (δ ppm): 9.90 (s, 1H), 7.75 (d, *J* = 8.2 Hz, 2H), 7.34 (d, *J* = 8.1 Hz, 2H), 2.33 (s, 3H); ^{13}C NMR (125 MHz, DMSO- *d*$_6$) (δ ppm): 192.99, 145.70, 134.55, 130.19, 130.07, 21.82.

4-Benzyloxybenzaldehyde (2q): 0.074g; Yield 85%; White solid; ^{1}H NMR (500 MHz, DMSO- *d*$_6$) (δ ppm): 9.83 (s, 1H), 7.83 (d, *J* = 7.7 Hz, 2H), 7.43 (d, *J* = 8.2 Hz, 2H), 7.37 (t, *J* = 7.7 Hz, 2H), 7.32 (d, *J* = 7.7 Hz, 1H), 7.17 (d, *J* = 8.0 Hz, 2H), 5.18 (s, 2H); ^{13}C NMR (125 MHz, DMSO- *d*$_6$) (δ ppm): 191.84, 163.83, 136.85, 132.34, 130.33, 129.05, 128.62, 128.39, 115.82, 70.20.

3-Phenoxybenzaldehyde (2r): 0.067g; Yield 78%; white solid; ^{1}H NMR (500 MHz, DMSO-d$_6$) (δ ppm): 9.91 (s, 1H), 7.63 (d, *J* = 7.5 Hz, 1H), 7.53 (t, *J* = 7.8 Hz, 1H), 7.40 (s, 1H), 7.36 (t, *J* = 7.6 Hz, 2H), 7.28 (d, *J* = 10.7 Hz, 1H), 7.17 – 7.09 (m, 1H), 7.02 (d, *J* = 8.7 Hz, 2H); ^{13}C NMR (125 MHz, DMSO-d$_6$) (δ ppm): 192.81, 158.21, 156.38, 138.49, 131.37, 130.71, 125.22, 124.83, 124.67, 119.75, 118.03.

Acetophenone (4a): 0.060g; Yield 68%; transparent liquid; ^{1}H NMR (500 MHz, DMSO- *d*$_6$) (δ ppm): 7.92 (d, *J* = 7.8 Hz, 2H), 7.59 (t, *J* = 7.9 Hz, 1H), 7.48 (t, *J* = 7.8 Hz, 2H), 2.53 (s, 3H); ^{13}C NMR (125 MHz, DMSO- *d*$_6$) (δ ppm): 198.44, 137.34, 133.68, 129.18, 128.67, 27.18.

4-Fluoroacetophenone (4b): 0.065g; Yield 73%; pale yellow liquid; ^{1}H NMR (500 MHz, DMSO- d$_6$) (δ ppm): 7.98 (dd, J = 8.8, 5.4 Hz, 2H), 7.27 (t, J = 8.8 Hz, 2H), 2.51 (s, 3H). ^{13}C NMR (125 MHz, DMSO- d$_6$) (δ ppm): 197.02, 165.56 (d, J = 251.6 Hz), 134.07 (d, J = 3.0 Hz), 131.68, 131.60, 116.21, 116.03, 27.12.

2,4-Difluoroacetophenone (4c): 0.067g; Yield 74%; white solid; ^{1}H NMR (500 MHz, DMSO- *d*$_6$) (δ ppm): 7.89 – 7.80 (m, 1H), 7.33 – 7.25 (m, 1H), 7.13 (td, *J* = 8.4, 1.6 Hz, 2H), 2.50 (s, 3H); ^{13}C NMR (125 MHz, DMSO- *d*$_6$) (δ ppm): 194.38, 166.62,166.62, 164.60, 164.50, 163.69, 163.58, 161.648, 161.542, 133.01,132.98, 132.93, 132.90, 122.81, 122.78, 122.71, 122.68, 112.78, 112.75, 112.60, 112.58, 105.73, 105.52, 105.30, 31.21.

4-Chloroacetophenone (4d): 0.067g; Yield 75%; transparent liquid; ^{1}H NMR (500 MHz, DMSO- *d*$_6$) (δ ppm): 7.89 (d, *J* = 8.6 Hz, 2H), 7.49 (d, *J* = 8.6 Hz, 2H), 2.51 (s, 3H); ^{13}C NMR (125 MHz, DMSO- *d*$_6$) (δ ppm): 197.31, 138.66, 135.92, 130.52, 129.22, 27.12.

2,4-Dichloroacetophenone (4e): 0.068; Yield 74%; white solid; ^{1}H NMR (500 MHz, DMSO- *d*$_6$) (δ ppm):7.68 (d, *J* = 8.4 Hz, 1H), 7.57 (d, *J* = 2.1 Hz, 1H), 7.45 (dd, *J* = 8.4, 2.0 Hz, 1H), 2.52 (s, 3H); ^{13}C NMR (125 MHz, DMSO- *d*$_6$) (δ ppm): 199.07, 137.53, 136.82, 131.54, 130.49, 128.20, 127.88, 30.85.

2-Bromoacetophenone (4f): 0.062g; Yield 68%; transparent solid; ^{1}H NMR (500 MHz, DMSO- *d*$_6$) (δ ppm): 7.64 (d, *J* = 7.8, Hz, 1H), 7.62 (d, *J* = 7.8, Hz, 1H), 7.43 (td, *J* = 7.5, 1.2 Hz, 1H), 7.40 – 7.33 (m, 1H), 2.52 (s, 3H); ^{13}C NMR (125 MHz, DMSO- *d*$_6$) (δ ppm): 201.31, 141.39, 134.08, 132.70, 129.62, 128.37, 118.32, 30.72.

3-Bromoacetophenone (4g): 0.067g; Yield 73%; yellow liquid; ^{1}H NMR (500 MHz, DMSO- *d*$_6$) (δ ppm): 8.00 (t, *J* = 1.8 Hz, 1H), 7.89 (d, *J* = 7.8 Hz, 1H), 7.76 (d, *J* = 7.9 Hz, 1H), 7.43 (t, *J* = 7.9 Hz, 1H), 2.53 (s, 3H). ^{13}C NMR (125 MHz, DMSO- *d*$_6$) (δ ppm): 197.26, 139.30, 136.24, 131.40, 131.19, 127.70, 122.65, 27.27.

4-Bromoacetophenone (4h): 0.063g; Yield 69%; light yellow solid; ^{1}H NMR (500 MHz, DMSO- *d*$_6$) (δ ppm): 7.83 (d, *J* = 6.6 Hz, 2H), 7.67 (d, *J* = 8.4 Hz, 2H), 2.52 (s, 3H); ^{13}C NMR (125 MHz, DMSO- *d*$_6$) (δ ppm): 197.65, 136.29, 132.26, 130.71, 127.83, 27.21.

3-Nitroacetophenone (4i): 0.069g; Yield 76%; yellow solid; ^{1}H NMR (500 MHz, DMSO- *d*$_6$) (δ ppm): 8.59 – 8.53 (m, 1H), 8.41 (dd, *J* = 8.3, 1.1 Hz, 1H), 8.33 (d, *J* = 7.6 Hz, 1H), 7.78 (t, *J* = 7.9 Hz, 1H), 2.64 (s, 3H); ^{13}C NMR (125 MHz, DMSO- *d*$_6$) (δ ppm): 197.01, 148.52, 138.41, 134.98, 131.11, 127.91, 122.91, 27.45.

3-Aminoacetophenone (4j): 0.072g; Yield 81%; brown solid; ^{1}H NMR (500 MHz, DMSO- *d*$_6$) (δ ppm): 7.12 – 7.05 (m, 3H), 6.76 (d, *J* = 6.5 Hz, 1H), 5.29 (s, 2H), 2.43 (s, 3H); ^{13}C NMR (125 MHz, DMSO- *d*$_6$) (δ ppm): 198.79, 149.51, 138.18, 129.61, 119.01, 116.47, 113.23, 27.20.

4-Aminoacetophenone (4k): 0.068g; Yield 77%; white solid; ^{1}H NMR (500 MHz, DMSO- *d*$_6$) (δ ppm): 7.64 (d, *J* = 7.0 Hz, 2H), 6.54 (d, *J* = 7.0 Hz, 2H), 5.96 (s, 2H),

10.57647/ijc.2026.1601.04

2.34 (s, 3H); ^{13}C NMR (125 MHz, DMSO- d_6) (δ ppm): 195.52, 154.15, 131.11, 125.44, 113.04, 26.35.

4-Hydroxyacetophenone (4l): 0.056g; Yield 63%; white solid; ^{1}H NMR (500 MHz, DMSO- d_6) (δ ppm):

10.31 (s, 1H), 7.79 (d, J = 8.8 Hz, 2H), 6.81 (d, J = 8.8 Hz, 2H), 2.42 (s, 3H);^{13}C NMR (125 MHz, DMSO- d_6) (δ ppm): 196.56, 162.54, 131.24, 129.12, 115.68, 26.73.

4-Methoxyacetophenone (4m): 0.065g; Yield 73%; yellow liquid; ^{1}H NMR (500 MHz, DMSO-d_6) (δ ppm): 7.87 (d, J = 8.4 Hz, 2H), 6.96 (d, J = 8.4 Hz, 2H), 3.78 (s, 3H), 2.46 (s, 3H); ^{13}C NMR (125 MHz, DMSO-d_6) (δ ppm): 196.78, 163.64, 130.94, 130.39, 114.24, 55.90, 26.75.

3,4-Dimethoxyacetophenone (4n): 0.063g; Yield 69%; pale yellow solid; ^{1}H NMR (500 MHz, DMSO- d_6) (δ ppm): 7.55 (dd, J = 8.4, 2.1 Hz, 1H), 7.38 (d, J = 2.1 Hz, 1H), 6.97 (d, J = 8.4 Hz, 1H), 3.78 (s, 3H), 3.76 (s, 3H), 2.47 (s, 3H); ^{13}C NMR (125 MHz, DMSO- d_6) (δ ppm): 196.79, 153.58, 149.07, 130.40, 123.54, 111.22, 110.67, 56.15, 55.91, 26.66.

4-Methylacetophenone (4o): 0.076g; Yield 86%; transparent liquid; ^{1}H NMR (500 MHz, DMSO- d_6) (δ ppm): 7.80 (d, J = 8.4 Hz, 2H), 7.26 (d, J = 8.5 Hz, 2H), 2.49 (s, 3H), 2.31 (s, 3H); ^{13}C NMR (125 MHz, DMSO- d_6) (δ ppm): 197.91, 144.00, 134.94, 129.71, 128.79, 27.04, 21.61.

3. Results and discussion

We explored metal catalysis and metal-associated transformation into a bioactive scaffold [17-21], thus further expanded the same via metallophotoredox decarboxylative oxygenation through visible-light-induced (LMCT) processes, with our continued interest in photocatalytic transformations [22], in decarboxylative oxygenation of aryl acetic acid, using iron(III)triflate as a photo redox catalyst (Scheme 1C).

Table 1. Optimization of the reaction conditions.[a]

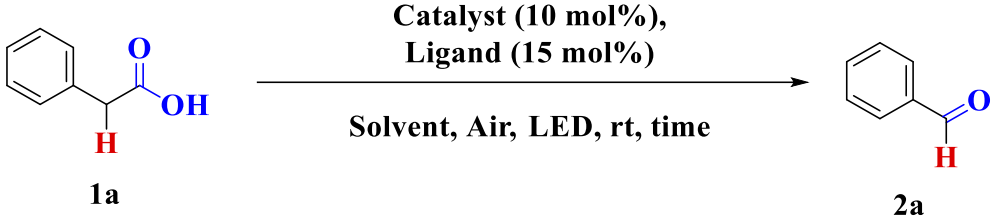

1a 2a

Entry	Catalysts	Ligand	LED lights	Air	Solvents	Time (hours)	Yield (%)
1	$FeCl_3.6H_2O$	Bpy	Blue (450 nm)	Open	ACN	12	NR
2	$Fe(NO_3)_3.9H_2O$	Bpy	Blue (450 nm)	Open	ACN	12	NR
3	$Fe(OTf)_3$	Bpy	Blue (450 nm)	Open	ACN	12	10
4	$Fe(OTf)_3$	Dtbpy	Blue (450 nm)	Open	ACN	12	14
5	$Fe(OTf)_3$	DMEDA	Blue (450 nm)	Open	ACN	12	26
6	$Fe(OTf)_3$	TMEDA	Blue (450 nm)	Open	ACN	12	70
7	$Fe(OTf)_3$	TMEDA	Blue (450 nm)	Open	ACN	8	68
8	$Fe(OTf)_3$	TMEDA	Blue (450 nm)	Open	ACN	24	70
9	$Fe(OTf)_3$	TMEDA	Blue (450 nm)	Open	Dioxane	12	34
10	$Fe(OTf)_3$	TMEDA	Blue (450 nm)	Open	NMP	12	45
11	$Fe(OTf)_3$	TMEDA	Blue (450 nm)	Open	DMA	12	67
12	$Fe(OTf)_3$	TMEDA	Blue (450 nm)	Open	Methanol	12	32
13	$Fe(OTf)_3$	TMEDA	Blue (450 nm)	Open	EtOAc	12	0
14	$Fe(OTf)_3$	TMEDA	Blue (450 nm)	Open	DCE	12	38
15	$Fe(OTf)_3$	TMEDA	Blue (450 nm)	Open	DCM	12	15
16	$Fe(OTf)_3$	TMEDA	Blue (450 nm)	Open	$CHCl_3$	12	10
17	$Fe(OTf)_3$	TMEDA	Violet (395 nm)	Open	ACN	12	65
18	$Fe(OTf)_3$	TMEDA	Purple (370 nm)	Open	ACN	12	54
19	$Fe(OTf)_3$	TMEDA	Green light (~525 nm)	Open	ACN	12	NR
20	$Fe(OTf)_3$	TMEDA	Red light (~630 nm)	Open	ACN	12	NR

[a]A Schlenk tube charged with iron(III) triflate (10 mol%, 0.10 equiv.), ligand (15 mol%, 0.15 equiv.), and phenyl acetic acid (0.7 mmol, 1 equiv.) in 3 mL solvent. The reaction mixture was stirred in open air and irradiated with a 10 W,~ 450 nm blue LED for 12 h; NR = no reaction

10.57647/ijc.2026.1601.04

In this protocol, iron(III)triflate acts as a catalytic initiator, promoting the activation of the carboxylic acid through LMCT to generate an aryl alkyl radical. This radical intermediate then undergoes oxidation to yield the corresponding aryl aldehyde.

The model reaction, involving phenylacetic acid (1a), was performed in acetonitrile using iron(III)triflate and different ligands to get product 2a. The mixture was irradiated with LEDs as the visible light source and stirred for 12 or more hours, as summarized in Table 1.

Reaction was conducted by taking iron(III) chloride hexahydrate, iron (III) nitrate nonahydrate ($Fe(NO_3)_3.9H_2O$), as a catalyst, and bypyridine (bpy) as a ligand in acetonitrile (ACN), but the reaction did proceed (entries 1 and 2, Table 1).

When the iron (III) triflate catalyst was used with the bpy ligand (entry 3, Table 1), the desired product was obtained in a poor yield of 10%. We got a 14% yield when we used ligand as 4,4′-di-tert-butyl-2,2′-bipyridine (dtbpy) (entry 4, Table 1). Further improvement in the yield up to 26% was observed in case N, N′-dimethylethylenediamine (DMEDA) as a ligand (entry 5, Table 1).

Further exploration of the ligand led to a 70% yield when N, N, N′, N′ -tetramethyl ethylenediamine (TMEDA) was used (entry 6, Table 1). While a reduction in the reaction time led to a lower yield, an increase in time did not improve the yield (entries 7 and 8, Table 1). Subsequent screening of alternative solvents failed to give expected results (entries 9 to 16, Table 1), which confirms that ACN is the most effective solvent for this transformation.

Further optimization was carried out to check the influence of different light wavelengths and reaction conditions. When the reaction was irradiated using violet light (395 nm), a moderate yield of 65% was obtained (entry 17, Table 1). A shift to purple light (370 nm) led to a decrease in yield to 54%, indicating that shorter wavelengths were less effective for this transformation (entry 18, Table 1).

Violet light (~390 nm): Gave a moderate yield of 66%, suggesting this wavelength is effective for promoting the reaction. While the use of green (~525 nm) and red light (~630 nm) did not afford the product, indicating that longer wavelengths are ineffective for initiating the photo redox process.

Different control experiments were conducted to evaluate the influence of various reaction parameters on the yield of product 2a. There was no reaction in the case of without a catalyst or without a ligand (entries 1-2, Table 2), indicating that the iron(III) triflate and the TMEDA ligand are essential for the reaction.

To confirm the necessity of light, a control experiment was performed in the absence of light (dark conditions), which resulted in no reaction, thereby confirming the photo-induced nature of the transformation (entry 3, Table 2).

Additionally, to assess the role of oxygen, the reaction was conducted under a closed inert atmosphere under N_2 and argon (entries 4 and 5, Table 2), where the reaction completely stopped compared to open-air conditions (entry 6, Table 2).

However, when the reaction was performed in a sealed system with an O_2 balloon, the yield significantly improved to 72% (entry 7, Table 2). This suggests that increased oxygen availability enhances the efficiency of the oxygenation step, making it a crucial parameter in optimizing the reaction outcome.

These results confirm the essential roles of the iron catalyst, ligand, light (particularly in the violet region), and molecular oxygen in enabling the decarboxylative oxygenation reaction. Additional experiments were conducted to explore the radical-mediated catalytic transformation of decarboxylative oxygenation using two equivalents of various reaction quenchers (entries 8–14, Table 2).

The addition of 2 equivalents of 2,2,6,6-tetramethylpiperidine-1-oxyl (TEMPO), butylated hydroxytoluene (BHT), or sodium ascorbate to the standard reaction of substrate 1a completely suppressed the reaction (entries 8–10, Table 2). A high-resolution mass spectrometry (HRMS) analysis revealed a TEMPO adduct (at M+H m/z = 248.2009), confirming the formation of a decarboxylative alkyl radical intermediate through visible light-induced ligand-to-metal charge transfer (LMCT) homolysis (Fig. 1).

The reaction was also fully inhibited in the presence of 2 equivalents of p-benzoquinone, indicating the involvement of a superoxide radical (Entry 11, Table 2). To probe the role of hydroxyl radicals, the reaction was conducted with tert-butanol, yielding product 2a in 67% yield (entry 12, Table 2), suggesting the absence of hydroxyl radicals.

To assess the involvement of singlet oxygen radicals, reactions were performed with 1,4-diazabicyclo[2.2.2] octane (DABCO), resulting in complete quenching of the reaction (entry 13, Table 2), while in the case of sodium azide (NaN3), it led to a minor yield of 2a (entry 14, Table 2).

These results confirm the participation of singlet oxygen radicals and support a single electron transfer (SET) mechanism in the reaction pathway. A plausible reaction mechanism for the photocatalytic decarboxylative oxygenation of aryl aliphatic carboxylic acid is proposed involving an organometallic complex of Fe3+, as presented in Fig. 2 [23].

Initially, an organometallic complex (i) was formed of Iron(III) triflate and TEMDA. The iron-ligand complex undergoes complexation with aliphatic carboxylic acid (1/3). Further Fe complex (ii) underwent a blue light-

mediated superoxide formation, which affords an alkyl radical via decarboxylation.

Further, the Fe complex (iii) led to the metathesis to afford alkyl hydroperoxide (vi), which transformed into aldehyde/ketone (2/4) product under the influence of blue light. We explored the substrate scope of the iron-mediated decarboxylative oxygenation reaction after obtaining suitable optimization conditions. Due to the presence of electron-donating and electron-withdrawing functional groups on substituted primary as well as secondary carboxylic acids, they had good sustainability, which promoted moderate to excellent yields.

We developed a series of carbonyl compounds from phenyl acetic acids (1a-r) to respective aldehyde (2a-r) in 62-85% yields.

The reaction was further explored using 2-pheylpropanoic acid (3a-o), which transformed into respective ketones (4a-o) in 63-86% yields (Table 3).

Table 2. Mechanistic studies with varying reaction conditions.[a]

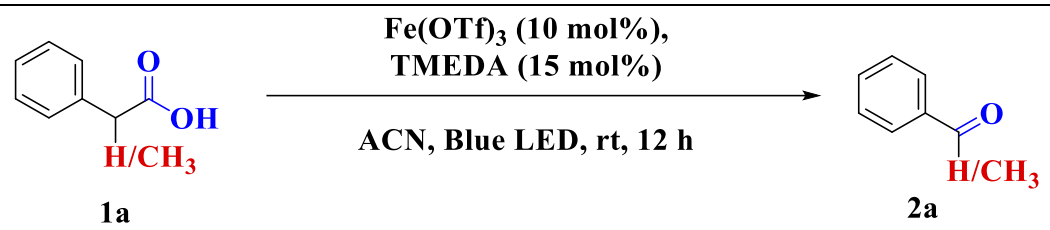

Entry	Variations from standard conditions	Yield 2a (%)	Entry	Quencher (2 equiv.)	Yield 2a (%)
1	Without $Fe(CF_3SO_3)_3$	ND	8	TEMPO	0
2	Without ligand	ND	9	BHT	0
3	Without light (in the dark)	ND	10	Sodium ascorbate	0
4	Under N_2 environment (without O_2)	ND	11	p-benzoquinone	0
5	Under an argon environment (without O_2)	ND	12	*tert*-butanol	67
6	Open air	70	13	DABCO	ND
7	Closed, O_2 Balloon	72	14	NaN_3	11

[a]A Schlenk tube charged with iron(III) triflate (10 mol%, 0.10 equiv.), ligand (15 mol%, 0.15 equiv.), and phenyl acetic acid (0.7 mmol, 1 equiv.) in 3 mL solvent. The reaction mixture was stirred in open air and irradiated with a 10 W,~ 450 nm blue LED for 12 h; NR = no reaction

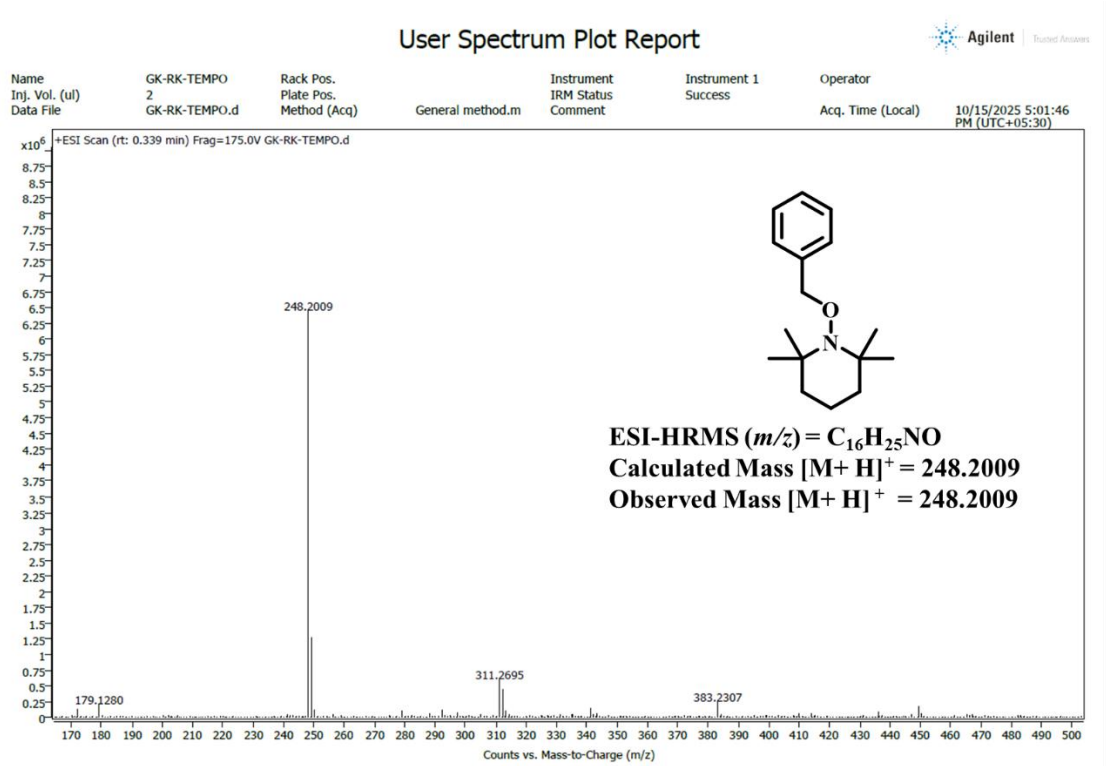

Figure 1. HRMS of TEMPO adduct

10.57647/ijc.2026.1601.04

Table 3. Substrate scope of iron-catalyzed decarboxylative oxygenation

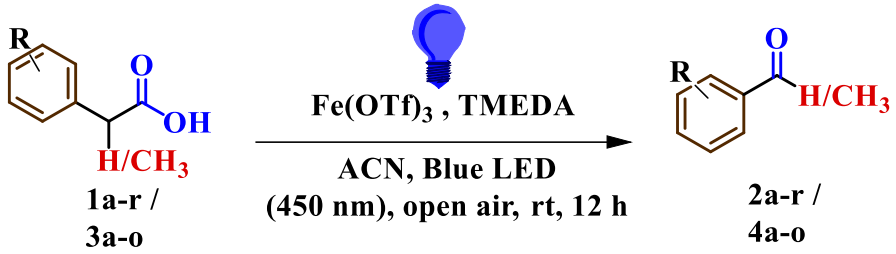

Product (2a-r) from aryl acetic acid (1a-r)	Yield (%)	Product (4a-o) from aryl propionic acid (3a-o)	Yield (%)
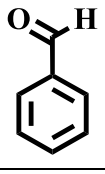 2a	70	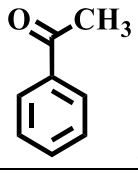 4a	68
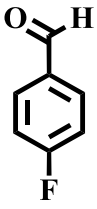 2b	69	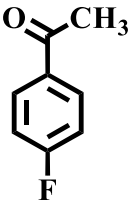 4b	73
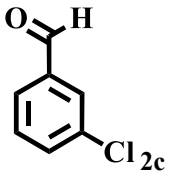 2c	76	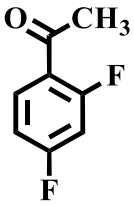 4c	74
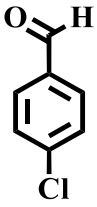 2d	73	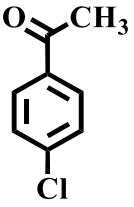 4d	75
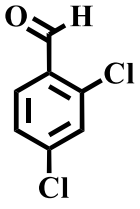 2e	70	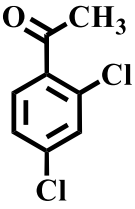 4e	74
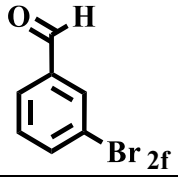 2f	66	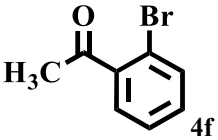 4f	68
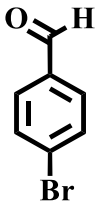 2g	62	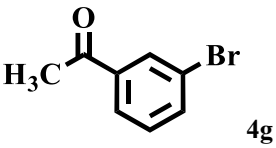 4g	73

Table 3. Substrate scope of iron-catalyzed decarboxylative oxygenation (continued…)

Product (2a-r) from aryl acetic acid (1a-r)	Yield (%)	Product (4a-o) from aryl propionic acid (3a-o)	Yield (%)
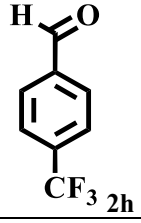 2h	72	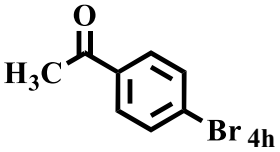 4h	69
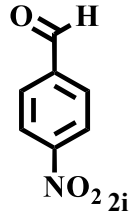 2i	64	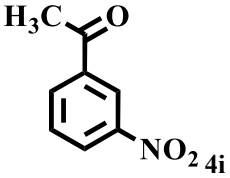 4i	76
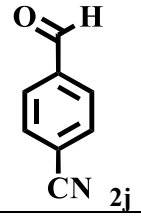 2j	64	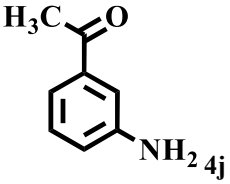 4j	81
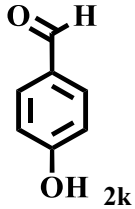 2k	78	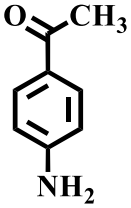 4k	77
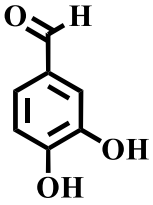 2l	68	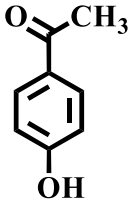 4l	63
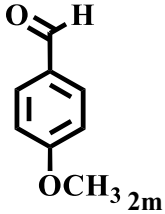 2m	67	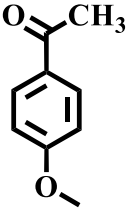 4m	73
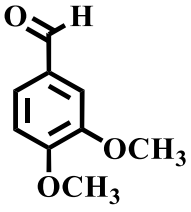 2n	67	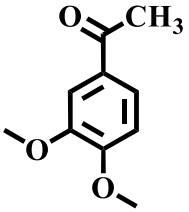 4n	69
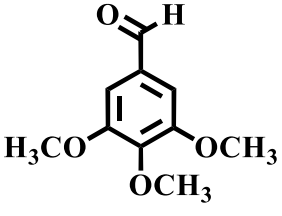 2o	68	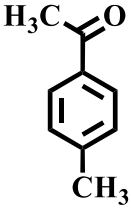 4o	86

Table 3. Substrate scope of iron-catalyzed decarboxylative oxygenation (continued…)

Product (2a-r) from aryl acetic acid (1a-r)	Yield (%)
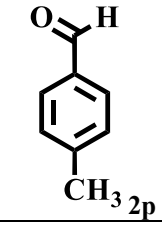 2p	77
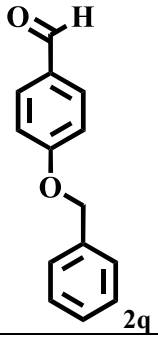 2q	85
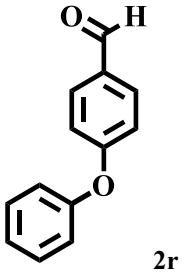 2r	78

[a]A Schlenk tube charged with iron(III) triflate (0.036 g, 10 mol%, 0.10 equiv), TMEDA (0.012 g, 0.016 ml, 15 mol%, 0.15 equiv), and phenylacetic acid /2-pheylpropanoic acid (0.7 mmol, 1 equiv.) in 3 mL of acetonitrile. The reaction mixture was stirred in open air and irradiated with a 10 W,~ 450 nm blue LED for 12 h.

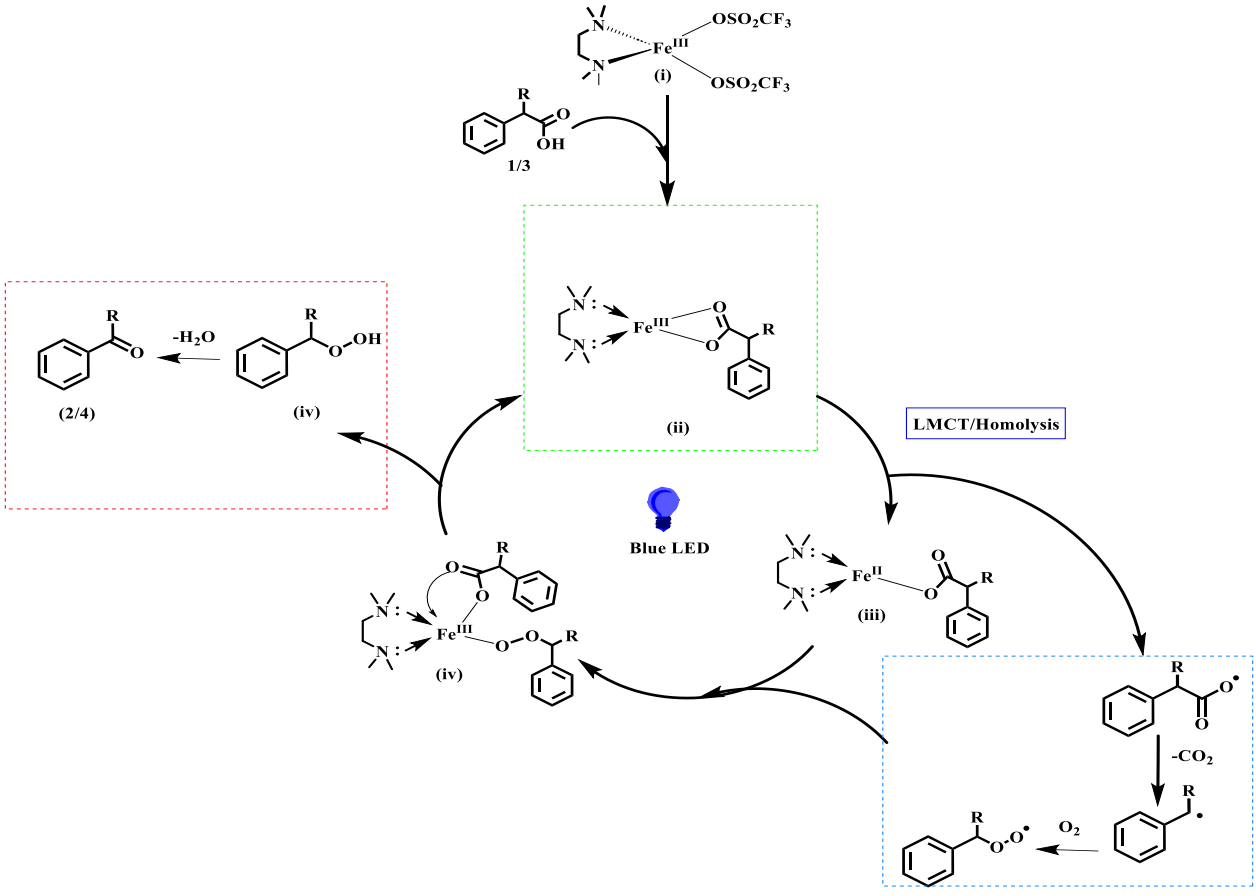

Figure 2. A plausible mechanism of the reaction

10.57647/ijc.2026.1601.04

4. Conclusion

Decarboxylative oxygenation of aryl acetic acids through visible light-induced ligand-to-metal charge transfer (LMCT) homolysis by using iron (III) triflate. This methodology demonstrated broad functional group tolerance and was effective, achieving good yields. We anticipate that this robust protocol will facilitate further exploration and application of carbonyl compounds in pharmaceutical development.

Acknowledgement

The authors acknowledge the Department of Pharmaceuticals, Ministry of Chemicals, and Fertilizers for the financial support.

Author Contributions
R.K. developed and synthesized the derivatives. S.K studied the reaction mechanism. G.L.K. hypothesized and supervised the work and writing the manuscript. All authors have given approval to the final version of the manuscript.

Data Availability Statement
The data associated with this research work is available in "Supporting Information".

Conflict of Interest
The authors declare no competing financial interest.

References

[1] C.W. Anson, S.S. Stahl, Chem. Rev. **120** (2020) 3749-3786. https://doi.org/10.1021/acs.chemrev.9b00717

[2] R. Guan, G. Chen, E.L. Bennett, Z. Huang, J. Xiao, Org. Lett. **25** (2023) 2482–2486. https://doi.org/10.1021/acs.orglett.3c00649

[3] A. Catalano, A. Mariconda, A.D. Amato, D. Iacopetta, J. Ceramella, M. Marra, C. Saturnino, M.S. Sinicropi, P. Longo, Organics **5** (2024) 395–428. https://doi.org/https://doi.org/10.3390/org5040021

[4] S. Geng, B. Xiong, Y. Zhang, J. Zhang, Y. He, Z. Feng, Chem. Commun. **55** (2019) 12699–12702. https://doi.org/10.1039/C9CC06584A

[5] B. Xiong, X. Zeng, S. Geng, S. Chen, Y. He, Z. Feng, Green Chem. **20** (2018) 4521–4527. https://doi.org/10.1039/C8GC02369G

[6] L.H.M. De Groot, A. Ilic, J. Schwarz, J. Am. Chem. Soc. **145** (2023) 9369–9388. https://doi.org/10.1021/jacs.3c01000

[7] Y. Pocker, B.C. Davis, J. Am. Chem. Soc. **95** (1973) 6216–6223. https://do.org/10.1021/ja00800a011

[8] T.B. Mete, T.M. Khopade, R.G. Bhat, Tetrahedron Lett. **58** (2017) 2822–2825. https://doi.org/10.1016/j.tetlet.2017.06.013

[9] K. Gholam Reza, A. Roxana, Chem. Res. Chinese Univ. **24** (2008) 464–468. https://doi.org/10.1016/S1005-9040(08)60097-5

[10] RS. Farhadi, P. Zaringhadam, R.Z. Sahamieh, Tetrahedron Lett. **47** (2006) 1965–1968. https://doi.org/10.1016/j.tetlet.2006.01.082

[11] M. Araghi, F. Bokaei, Polyhedron **53** (2013) 15–19. https://doi.org/10.1016/j.poly.2013.01.052

[12] Y. Sakakibara, P. Cooper, K. Murakami, K. Itami, Chem. - An Asian J. **13** (2018) 2410–2413. https://doi.org/10.1002/asia.201800529

[13] T.M. Faraggi, W. Li, D.W.C. MacMillan, Isr. J. Chem. **60** (2020) 410–415. https://doi.org/10.1002/ijch.201900130

[14] S. Shirase, S. Tamaki, K. Shinohara, K. Hirosawa, H. Tsurugi, T. Satoh, K. Mashima, J. Am. Chem. Soc. **142** (2020) 5668–5675. https://doi.org/10.1021/jacs.9b12918

[15] J.L. Tu, H. Gao, M. Luo, L. Zhao, C. Yang, L. Guo, W. Xia, Green Chem. **24** (2022) 5553–5558. https://doi.org/10.1039/d2gc01738e

[16] F.N. Castellano, J. Rehbein, O. Reiser, ChemComm **58** (2022) 4456–4459. https://doi.org/10.1039/d2cc00570k

[17] R. Bashary, G.L. Khatik, Bioorg. Chem. **82** (2019) 156–162. https://doi.org/10.1016/j.bioorg.2018.10.010

[18] L. Chandrakar, R. Ambatwar, G.L. Khatik, J. Mol. Struct. **1296** (2024) 136817. https://doi.org/https://doi.org/10.1016/j.molstruc.2023.136817

[19] S. Kumar, N. Bhanwala, J. Malik, K. Jagrati, G.L. Khatik, Res. Chem. Intermed. **50** (2024) 4387–4405. https://doi.org/10.1007/s11164-024-05360-z

[20] M. Devi, P. Kumar, R. Singh, J. Sindhu, R. Kataria, Eur. J. Med. Chem. **250** (2023) 115230. https://doi.org/https://doi.org/10.1016/j.ejmech.2023.115230

[21] V. Gupta, N.S. Sundaramoorthy, N. Bhanwala, R. Ambatwar, S. Kumar, R. Singh, G.L. Khatik, J. Comput. Biophys. Chem. **23** (2024) 1197–1208. https://doi.org/10.1142/S2737416524500388

[22] N. Bhanwala, N.S. Sundaramoorthy, S. Gollapudi, A. Sharma, R. Singh, G.L. Khatik, Med. Chem. Res. **33** (2024) 1926–1937. https://doi.org/10.1007/s00044-024-03295-z

[23] L. Ellouzi, I., Regraguy, B., El Hajjaji, S., Harir, M., Schmitt-Kopplin, P., Lachheb, H., & LaÃ¢nab, Iran. J. Catal. **12** (2011). https://doi.org/https://doi.org/10.30495/ijc.2022.1941684.1875

[24] M. Innocent, G. Lalande, F. Cam, T. Aubineau, A. Guérinot, European J. Org. Chem. **26** (2023) e202300892. https://doi.org/10.1002/ejoc.202300892